Brazilian Journal of Physics
ISSN: 0103-9733
luizno.bjp@gmail.com
Sociedade Brasileira de Física
Brasil

Kaci, Meziane; Ait Said, Hakim; Laifaoui, Abdelkrim; Aissou, Massinissa; Nouri, Hamou; Zebboudj, Youcef

Investigation on the Corona Discharge in Blade-to-Plane Electrode Configuration

Brazilian Journal of Physics, vol. 45, núm. 6, 2015, pp. 643-655
Sociedade Brasileira de Física
São Paulo, Brasil

Braz J Phys (2015) 45:643–655
DOI 10.1007/s13538-015-0357-4

SOCIEDADE BRASILEIRA DE FÍSICA

GENERAL AND APPLIED PHYSICS

Investigation on the Corona Discharge in Blade-to-Plane Electrode Configuration

Meziane Kaci[2] · Hakim Ait Said[1,2] · Abdelkrim Laifaoui[2] · Massinissa Aissou[2] · Hamou Nouri[2] · Youcef Zebboudj[2]

Received: 1 May 2015 / Published online: 19 October 2015

Abstract The aim of this work is to analyze the characteristics of the corona discharge in blade-to-plane electrode configuration. An experimental investigation has been carried out on the geometric parameters that govern the formation of both positive and negative corona discharges, such as the inter-electrode distance, the blade-to-blade spacing, and the number of the discharging blades. The current-voltage characteristics, the breakdown voltage, and the Warburg current distribution were measured. The assisted corona discharge is an example of a blade electrode discharge that can be used to reduce the operating voltage of a conventional corona discharge. The current-voltage characteristics of both positive and negative corona discharges in a blade-to-plane electrode configuration are of the Townsend's law form. The general formula proposed by Meng et al. can also be applied in this system. It has been shown that the breakdown voltage and the corona conductance are strongly affected by the inter-electrode distance. To obtain a maximum current, the blade electrodes should be distant from each other by a value of $2a \geq h$. To obtain a constant value of current, the blade electrodes should be separated by a value of $2a >> h$, confirming the Cooperman's law. The current density distribution is satisfied; an exponent of 5.0 is taken for positive polarity and an exponent of 4.8 for negative polarity.

✉ Hakim Ait Said
hakimdoz@yahoo.fr

[1] Département de Génie Electrique, Institut des Sciences et de Technologie, Centre Universitaire A-Zabana de Relizane, Relizane, Algeria

[2] Laboratoire de Génie Electrique, Faculté de Technologie, Université A-Mira Targa Ouzzemour, Bejaia 06000, Algeria

Keywords Corona discharge · Inter-electrode distance · Blade-to-blade spacing · Current-voltage characteristics · Breakdown voltage · Current density distribution

1 Introduction

Corona discharge has been extensively used in different applications such as electrostatic precipitator, electricity production, electro-photography, electrostatic separator, neutralization, and electrostatic painting [1–7]. The electric corona discharge usually occurs when a high voltage is applied between two electrodes with substantially different radii of curvature [8, 9]. The high electric field at the vicinity of the corona electrode causes gas ionization and partial breakdown. While the whole process is rather complicated, the ions of the same polarity of the corona electrode are drifting to the other electrode. A space charge is formed and an electric current flows between both electrodes [10, 11]. The displacement of ions is congested by very high frequency collisions with electrically neutral air molecules. Complete momentum transfer from the ionic space charge to the air bulk can be supposed to take place. Therefore, the Coulomb force acting on the ions becomes an electric body force on the air molecules. The current that is usually carried out by corona discharge flows from a high-voltage electrode and ionizes the inter-electrode air to create plasma around the active electrode. This happens when the geometrical configuration of the electrodes includes an electrode of sharp tip such as point-to-plane, point-to-grade, wire-to-plane, bipolar wires-to-plane, spike-plate multi-electrode, wire-cylinder, and blade-plane electrodes [12–18]. Interpreting the idea of wire and point geometries, we opted for union of the two electrodes in order to achieve a blade. Besides, the idea of the blade-plane geometry is inspired from the experiments that have been made for the point-plane and

wire-plane geometries, as in the blade-plane configuration, the electric field in the vicinity of the blade is intense thanks to its radius of curvature. This geometry facilitates the orientation of the field lines towards the collection plan, which enables a high energy. If the voltage of the active electrode (blade) is large enough, the air at the blade tip ionizes and becomes conductive which leads to the formation of a highly curved region on electrodes. The corona discharge is therefore associated with non-uniform electric field. The type of corona is determined by the polarity of the active electrode. If the voltage of the blade is positive with respect to the plane electrode, the corona is said to be positive corona while it is called negative corona, when the blade is in negative voltage. The current-voltage characteristics of corona discharge for positive and negative polarities are not the same because the bulk and velocity between electrons and charge ions are different. The current-voltage characteristics in corona discharge have been described by several empirical formulas involving different geometrical configurations of electrodes [12, 13, 19–22].

In this work, the results of an experimental investigation into the current-voltage characteristics, conductance parameters, and current density distribution of DC corona discharge in blade-to-plane electrode configuration have been presented. A blade-plane configuration was used with inter-electrode spacing in a range of 20–50 and 100–130 mm. The whole experiments were carried out in open air with a relative air density δ=1.

2 Theory of Corona Discharge

2.1 Current-Voltage Characteristics

A stable corona discharge is characterized by a nonlinear relationship between the corona current and the applied voltage. The relationship between the corona current and the applied voltage can be expressed by a theoretical simple law for the case of wire-to-cylinder electrode configuration [19, 20] and derived for the case of wire-to-plane electrode configuration by Cooperman [23]. After that, it was found that the Townsend's law could also be used somewhere for point-to-plane electrode configuration, as Henson divulged [21]. This formula is given by:

$$I = KV(V-V_0) = KV^2-KV_0V \tag{1}$$

where I is the corona current, V is the corona applied voltage, V_0 is the corona onset voltage, and K is a dimensional constant that depends on the geometric parameters of the setup and the charge carrier mobility in the drift region.

The mathematical analysis of the experimental data and the application of corona threshold allow us to modify the Townsend relation. A new general formula in characterizing the relationship of the corona current-voltage was derived and expressed by Meng et al. [12] as follows:

$$I = A(V-V_0)^n \tag{2}$$

$$\log_{10}(I) = n\cdot\log_{10}(V-V_0) + b;\ A = 10^b \tag{3}$$

It was demonstrated that the exponent n falls into a limited scope of 1.5–2.0. This formula can well explain the inconsistencies met by other existing formulae and best represent the corona current-voltage characteristics with a suitable accuracy.

2.2 Warburg's Law and Current Density

There is one aspect of DC corona discharge in air that is of special interest, namely the distribution of ionic current density on the plane, which for the case of a point-to-plane configuration has been experimentally demonstrated to fit the following relationship, known as Warburg's law [24]:

$$J(x) = J(\theta) = J(0)\cos\theta^m, \tag{4}$$

where θ is the angle at the discharge active electrode, between the perpendicular and the probe on the collecting plate, $J(0)$ is the current density directly under the discharge active electrode, and m is a parameter determined by curve fitting. Warburg found that m values are 4.65 and 4.82 for negative corona and positive corona discharges, respectively. The power m varies according to the configuration and dimensions of the electrodes. The current density distribution measurements given by Hara et al. [25] in wire-to-plane geometry are satisfied for an exponent m=4.8 according to the wire diameter and inter-electrode spacing.

Carreno [26] found, for the low heights, $h\leq$16 mm, in a wire-to-plane electrode configuration, the same empirical relationship which describes the current density, with m varying from 4.2 to 5.98. Zebboudj et al. [27] have measured the current density and the electric field, with the linear probe, at the passive electrode in wire-to-plane configuration. The blade-to-plane electrode configuration is described as an assembly between point-to-plane and wire-to-plane. In this geometry, the results obtained of the m parameter will be compared with [24], [25], and [27].

In this work, the Warburg's law is also derived from the measurements. The probe collector (P) is also used to measure the normal current density J when the probe is unbiased [28]:

$$J = \frac{I_0}{\pi r_m^2} \tag{5}$$

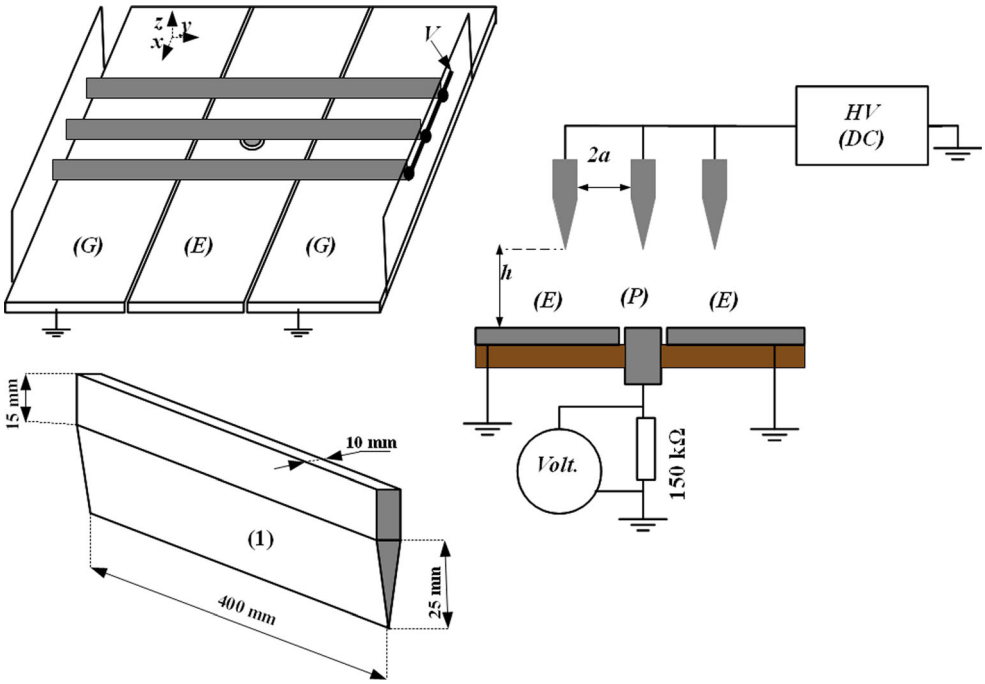

Fig. 1 Schematic of the experimental setup, including the relevant geometric parameters and the electrical circuit. *G* guard planes, *P* probe, *E* electrode

where r_m=2.25 mm is the effective radius of the probe and I_0 the collected current of corona discharge.

2.3 Peek's Law and the Onset Voltage

The corona onset voltage V_0 is the applied voltage required to attain the critical electric field necessary for the ionization of the air molecules near the surface of the wire or point. Peek's law [29] relates this onset voltage to the gap distance h as a function of the radius of curvature r and the interstitial gas pressure P and temperature T [30, 31]. For a wire-to-plane corona, this relationship is:

$$E_0 = m_v g_0 \delta \left(1 + \frac{0.0308}{\sqrt{\delta r}}\right) \tag{6}$$

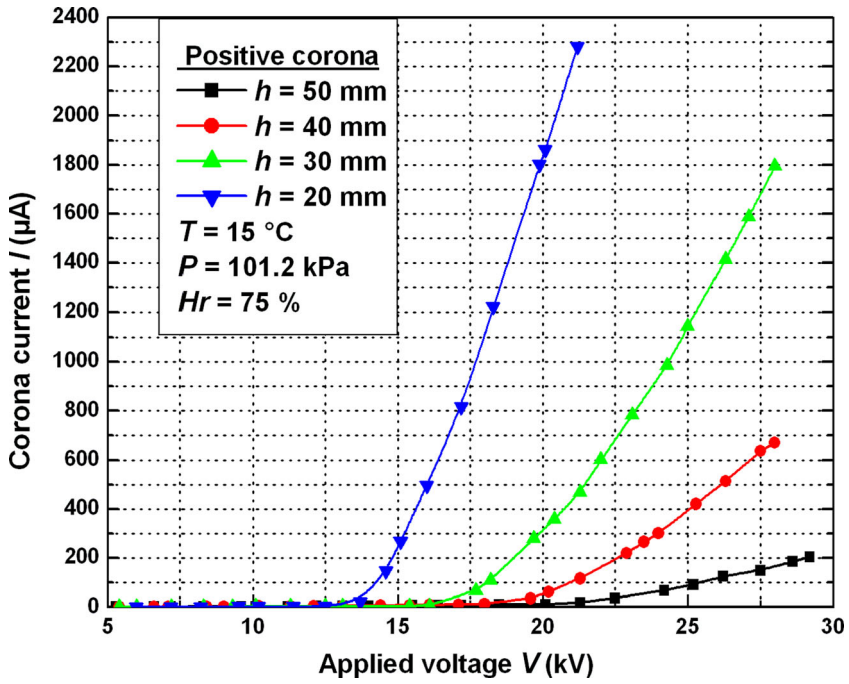

Fig. 2 Effect of inter-electrode distance on positive corona current-voltage characteristics

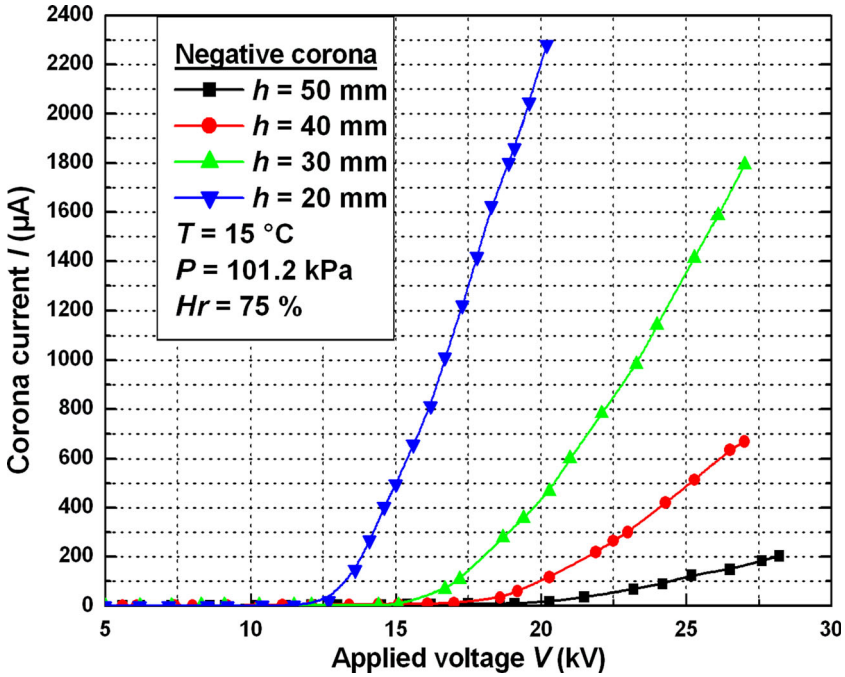

Fig. 3 Effect of inter-electrode distance on negative corona current-voltage characteristics

Thus, the onset voltage can be estimated by using the formula [30]:

$$V_0 = E_0 \times r \times ln\left(\frac{h}{r}\right) \tag{7}$$

When the number of wires is high, the geometry can be considered equivalent to a coaxial system as described by Cooperman [23], where the equivalent radius R_e is given by:

$$\text{for} \quad \frac{h}{a} \leq 0.6 \quad r = R_e = \frac{4h}{\pi} \tag{8}$$

$$\text{for} \quad \frac{h}{a} \geq 2.0 \quad r = R_e = \frac{a}{\pi} e^{\pi h/2a} \tag{9}$$

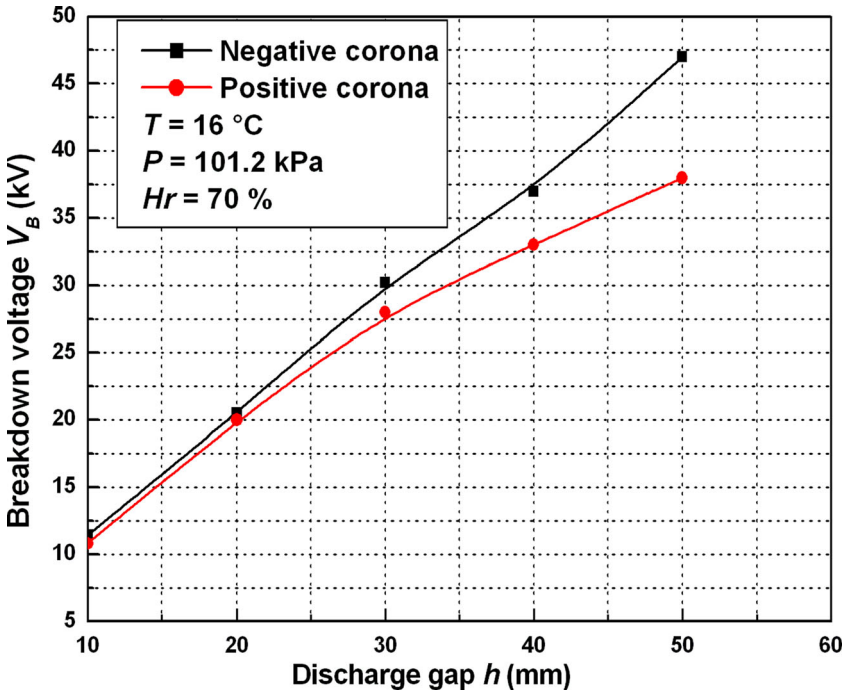

Fig. 4 Experimental breakdown voltages at various discharge gaps

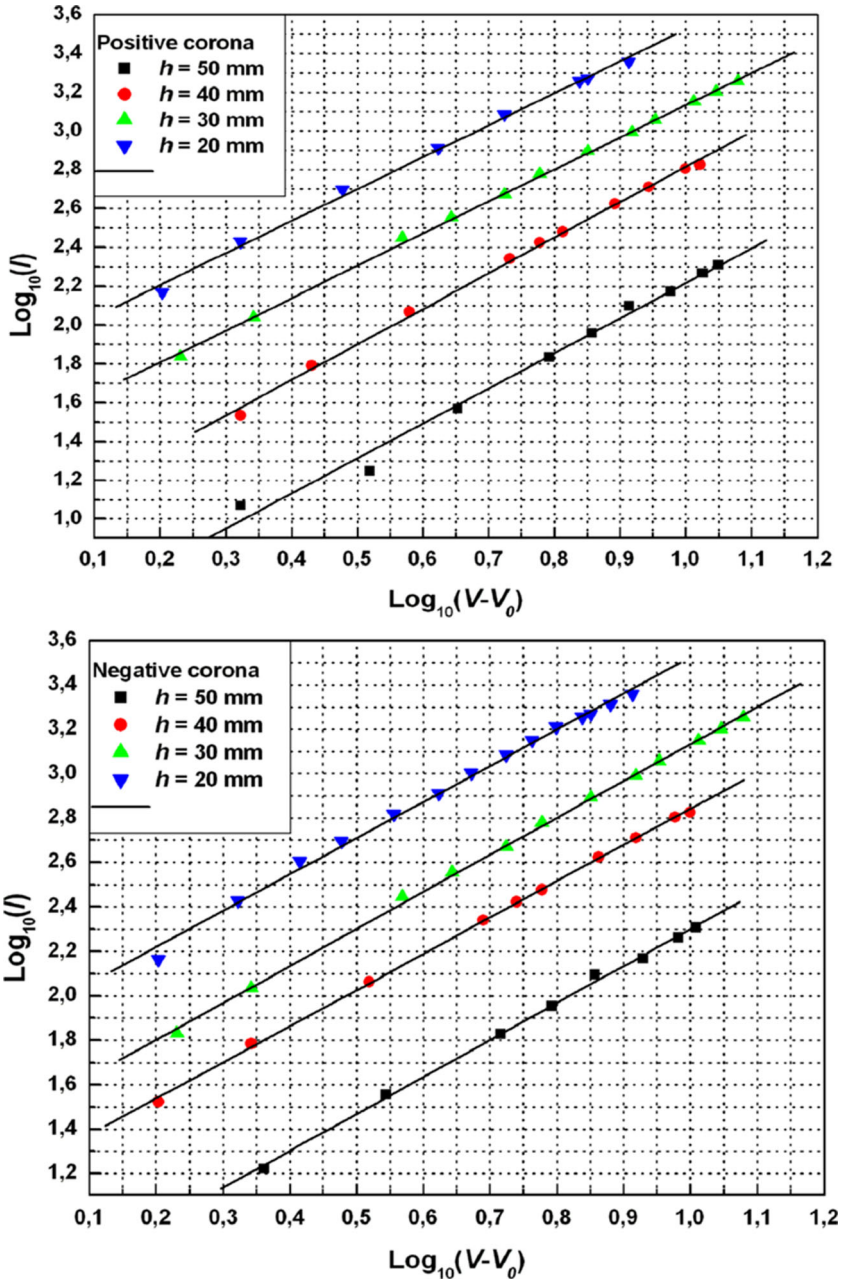

Fig. 5 The dependence of both positive and negative corona current (I: μA) versus the voltage difference ($V-V_0$, kV) on a log scale, at various discharge gaps; the *solid lines* are least square fitting lines

The parameter δ is the air density factor based on pressure and temperature and is given by:

$$\delta = \frac{3.92P}{273 + T} \tag{10}$$

where P is the pressure given in centimeters of mercury, and T is the temperature in degrees Celsius. Other quantities appearing in Eqs. (6)–(9) are as follows: m_v is an irregularity factor to account for the condition of the wire, r is the radius of curvature of the wire, h is the distance between the wire and the plate, a is the half wire-to-wire spacing, and g_0 is the disruptive critical voltage gradient, of the order of 30 or 27.2 kV/cm, for air [31, 32]. For ideal smooth wires, m_v=1, but practically m_v varies from 0.85 to 0.98, depending on the wires condition.

Table 1 Results of exponent n for various discharge gaps

h (mm)	50	40	30	20
n				
Negative corona	1.65	1.66	1.82	1.8
Positive corona	1.63	1.66	1.63	1.67

3 Experimental Procedure

The experimental setup in this study is illustrated in Fig. 1. This system consists of an aluminum blade (corona active electrode) with a radius of curvature r=0.019 mm and stainless steel planes (corona passive electrode). The end-effects were prevented by the two guard planes (G). The three parallel blades are fixed with two insulating supports and the circular probe (P) is incorporated on a same level of surface at the center of the biased electrode (E). All the components are made of stainless steel and are fixed with insulating probes. Positive or negative direct voltage, of a 0 to ±140 kV source (HV), is applied to the blades. A high-voltage divider and a DC voltmeter are used to measure the applied voltage V. The corona current is measured via the potential drop across the resistance 150 kΩ with the DC digital voltmeter. The plane (E) has a width equal to l=200 mm according to the y-axis and a length equal to L=400 mm according to the x-axis. The inter-electrode distance varies from 20 to 50 mm, and the blade-to-blade spacing varies from 20 to 50 mm and 100 to 130 mm, with almost a 10-mm increment.

A digital video camera is utilized to record simultaneously the indications of the two digital voltmeters used for the

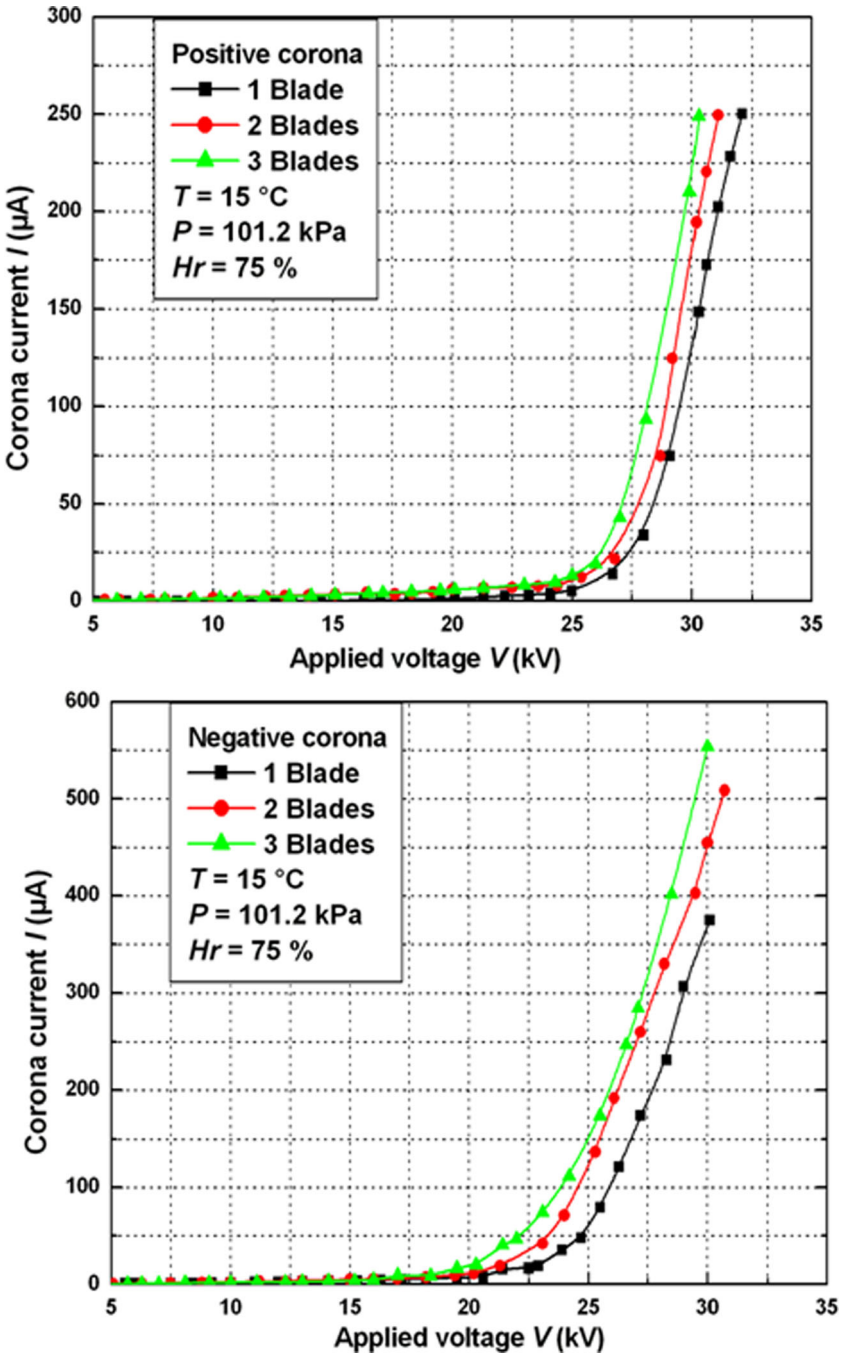

Fig. 6 Measured positive and negative corona current-voltage characteristics for various numbers of discharging blades, h=50 mm and 2a=40 mm

measurements respectively for the applied voltage and the corona current [33]. The applied voltage V rises gradually from the value V_1 to the value V_2 such as $V_1<V_0<V_2$, where V_0 is the corona onset voltage and V_2 is the inferior corona voltage at the breakdown voltage. The playback of the video recording can easily restore the values of corona current and the applied potential in order to draw the current-voltage characteristics. This direct registration procedure for current-voltage characteristics has several advantages. The stability of the discharge test interval corona can be quickly checked from the reproducibility of the characteristic.

4 Results and Discussion

4.1 Current-Voltage Characteristic Measurements

4.1.1 Effect of the Blade-to-Plane Spacing

Figures 2 and 3 show the current-voltage characteristics from corona onset to the occurrence of spark with inter-electrode spacing in the 20–50 mm range for both positive and negative corona discharges. Before onset, the currents measured were of the order of a nA signifying noise, and the currents increased to the order of a μA after onset. Generally, the results are as expected, when the electrode gap decreases, the onset voltage decreases and the magnitude of the corona current increases. It was also observed that the range of stable operating voltages decreased as the electrode gap decreased. This is driven by both the onset voltage and the spark-over voltage. The DC current through the inter-electrode gap is a nonlinear function of the applied voltage [19]. Townsend's first ionization coefficient, which denotes the number of electrons produced over a distance of h traveled by a single electron in the direction of the applied voltage, increases with increasing electronic energy. The onset voltage increases at a high inter-electrode distance for both positive and negative corona discharges, which was in agreement with the prediction of Peek formula [32].

The electric breakdown voltage is defined in gases as the potential between two electrodes which provides a stationary electric current in a gas located in a space between two electrodes (blade-plane). Basing on the condition of existence of an electric current in a gas between two electrodes separated by a distance, h=10 to 50 mm. In our system, the origin dynamics of an electric current may have various mechanisms. Therefore, the electric breakdown is considered as a multiplication of electron avalanches where an individual avalanche and a circle of processes of electron and ion production start from formation of secondary electrons at the cathode and finish by attachment of led electrons to the anode. Along with this electric breakdown mechanism, the streamer mechanism is possible and dominates at large distances between electrodes, $h\geq$10 mm [34, 35], as shown in Fig. 4.

With the objective to characterize the relationship of the corona current-voltage, a new general formula in characterizing was derived and expressed in Eq. (2), as described by Meng et al. [12]. The I-V characteristics of the blade-plane system appear also to follow the general formulae proposed by Meng et al., given by Eq. (2), where the parameter n can be determined by the Eq. (3), shown in Fig. 5 for both DC positive and negative coronas. The influence of the inter-

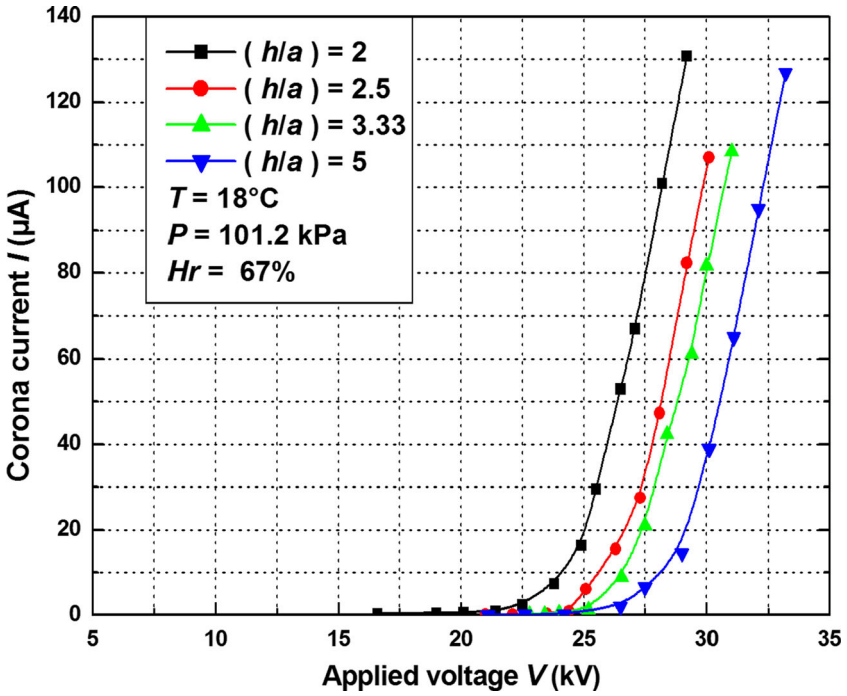

Fig. 7 Effect of blade-to-blade spacing on negative corona current-voltage characteristics at h=50 mm

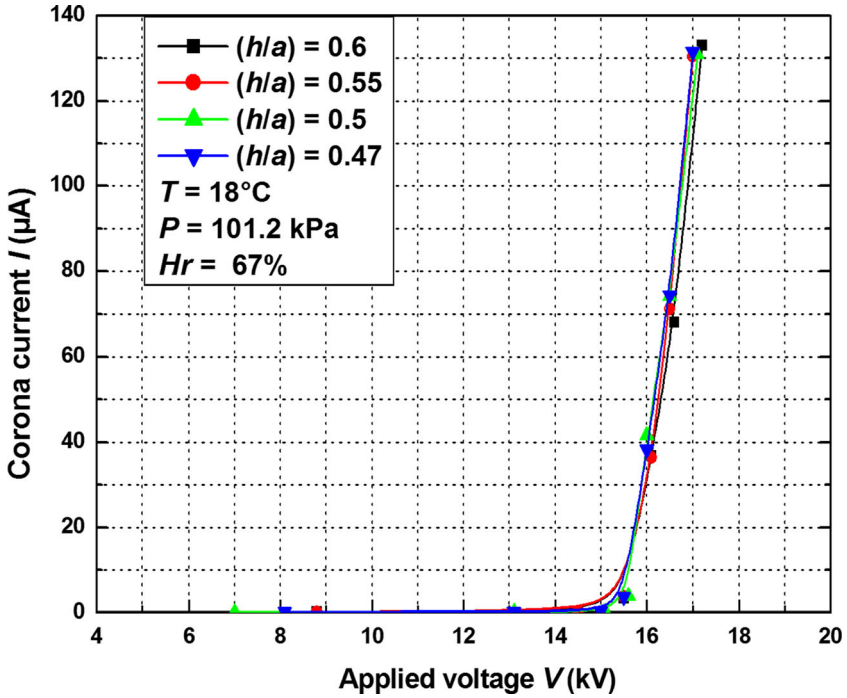

Fig. 8 Effect of blade-to-blade spacing on negative corona current-voltage characteristics at h=30 mm

electrode distance on the values of the parameter n is shown in Table 1. It is noticed that the value of the exponent n falls into a limited scope from 1.63 to 1.82. Moreover, it was demonstrated that the formula is applicable not only for both negative and positive corona discharges in point-to-plane geometries but also for both polarities in blade-to-plane geometries. With the optimal exponent n, the formula can also explain the inconsistencies met by other existing formulae and best represent the corona current-voltage characteristics with a good accuracy [12].

4.1.2 Effect of the Blade-to-Blade Spacing

The experimental data for various numbers of discharging blades are summarized in Fig. 6, for both positive and negative corona discharges, in the form $I=f(V)$. They all follow the

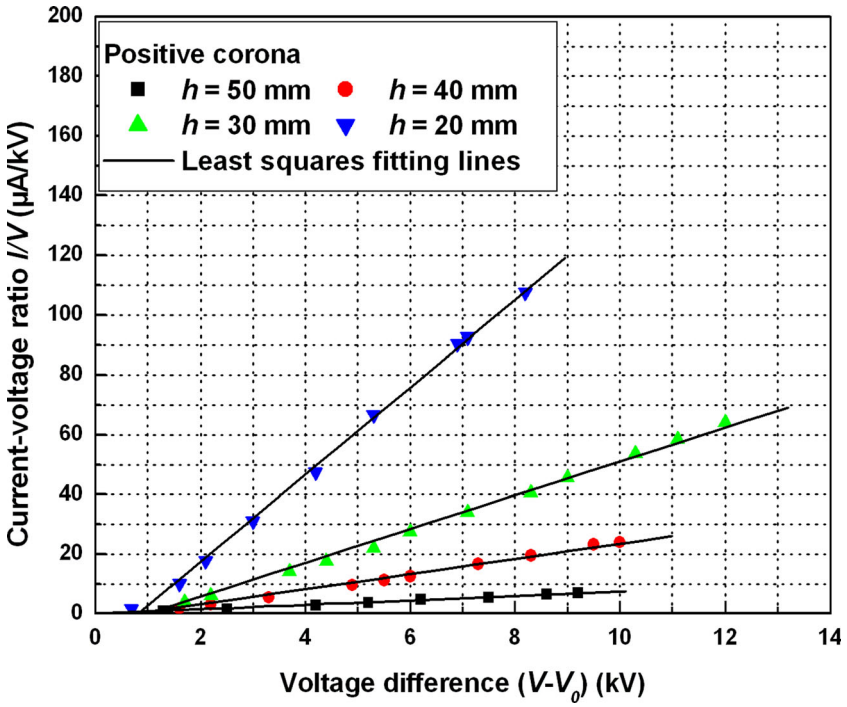

Fig. 9 Positive corona conductance characteristics for various inter-electrode distances

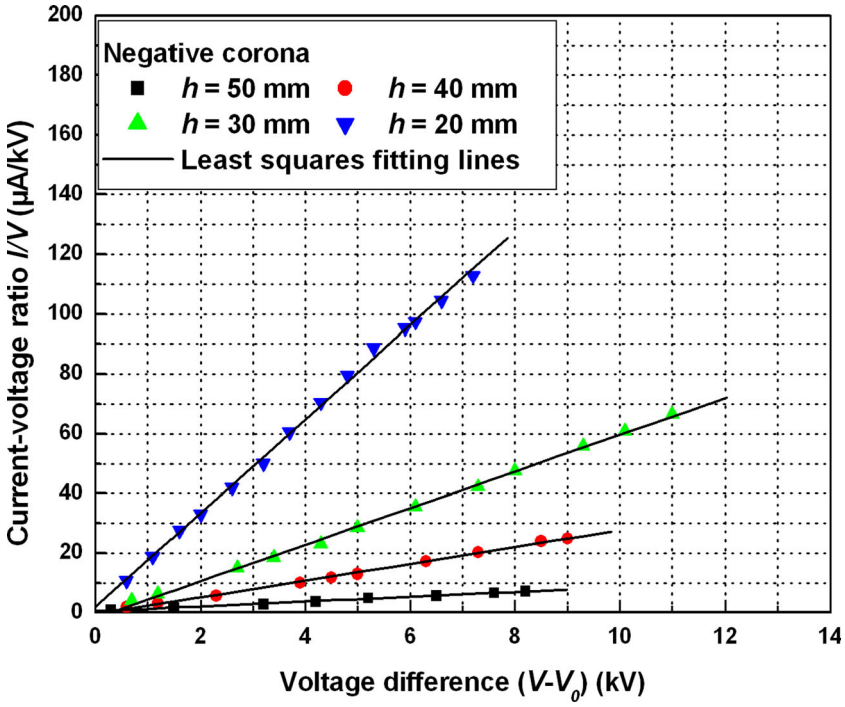

Fig. 10 Negative corona conductance characteristics for various inter-electrode distances

quadratic Townsend's law. The measured *I-V* characteristics of the negative corona discharge are always higher than those measured from the positive ones. The current values of the negative corona discharge are higher than those of the positive ones for the same applied voltage and the same number of discharging blades.

Figures 7 and 8 show the effect of interspacing $2a$ on the corona current under negative DC voltage. The longer is the interspacing, the higher is the corona current at the same applied voltage, as is shown in Fig. 7. This trend is attributed to the weakness of the interaction between space charges in the discharge cone under each electrode tip, which increases the possibility of streamer growth because of increasing the maximum electric field. It is clearly seen that the corona current increases when increasing the blade-to-blade spacing $2a$ with a decrease of the onset voltage. To obtain a maximum current, the electrode blades should be $2a \geq h$ distant from one another, confirming the Cooperman's law, under the condition of Eq. (9). Figure 8 shows that the blade-to-blade spacing has not been an influence on the characteristic $I=f(V)$. The discharge current is the same whatever the blade-to-blade spacing (the same characteristic for different blade-blade spaces). In order to obtain a constant value of current, the blade electrodes should be at a distance of $2a>>h$, confirming the Cooperman's law, under the condition of Eq. (8).

4.2 Corona Conductance

The $(I/V)=f(V-V_0)$ diagrams are shown to be a good test on the validity of the nonlinear law, Eq. (1). The importance of the slope of the corona characteristics can be more clearly perceived by analyzing the corona conductance trends. The slope K together with the intercept V_0 with the baseline completely characterizes the glow region of the discharge. The ratio of the corona current I with V should produce straight lines since the current is proportional to $V(V-V_0)$. Figure 9 shows the positive corona conductance values calculated from the data in Fig. 2, and the corresponding corona conductance for negative polarity was calculated using the data in Fig. 3. The results are shown in Fig. 10. The calculated corona conductance slope value summary is given in Table 2. The values obtained at h=20, 30, 40, and 50 mm fit a straight line. For the longer gaps, there is a smaller deviation from the quadratic law. The experimental values of coefficient K for h= 50 mm can be compared with experimental measurements appearing in [33], which were measured at h=50 mm in a wires-to-plane corona discharge. The K values for both corona discharges in [33] are $K+=0.310$ nS/kV, $K-=0.332$ nS/kV and in this work are $K+=0.73518$ nS/kV, $K-=0.81079$ nS/kV. The corona conductance in blade-to-plane for both polarities is about 60 % higher. It is demonstrated that the effect of

Table 2 Results of corona conductance K for various discharge gaps

h (mm) K (nS/kV)	50	40	30	20
Positive corona ($K+$)	0.73518	2.5278	5.65859	14.64286
Negative corona ($K-$)	0.81079	2.81796	6.13848	15.7383
Ratio $K-/K+$	1.103	1.115	1.085	1.075

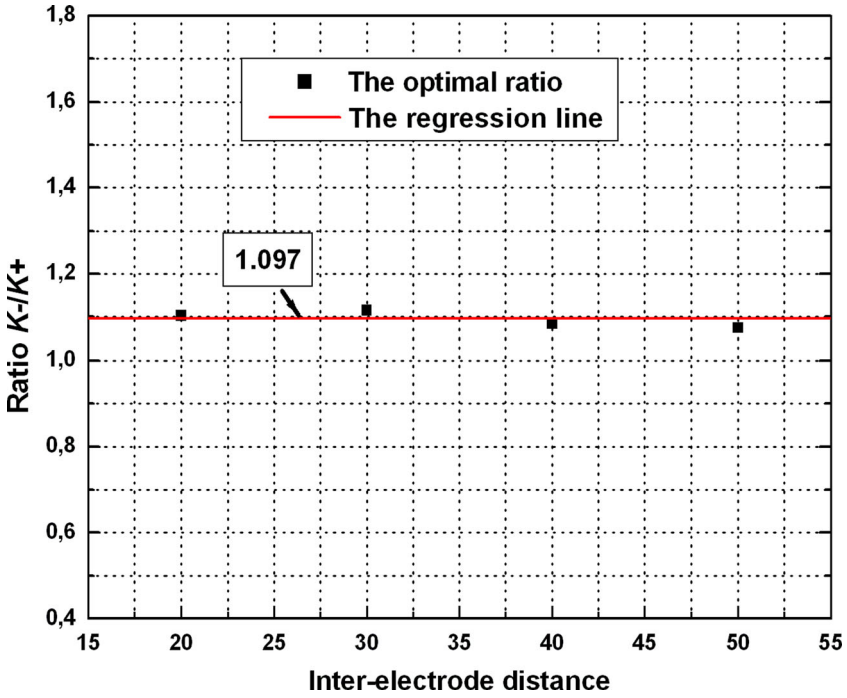

Fig. 11 Variation of the ratio ($K-/K+$) versus the inter-electrode distance

inter-electrode spacing on the conductance is very large, and the corresponding values in Table 2 are about 62 % higher.

The corona conductance K depends on the corona blade-to-plane spacing h and the charge carrier's mobility μ. For the same geometry, the ratio $K-/K+$ represents also the ratio $\mu-/\mu+$ of the charge carriers motilities. This ratio is practically independent on the corona blade-to-plane spacing, as it is clearly shown in Fig. 11. Moreover, it is always noted in literature that there is a minor difference between the motilities $\mu+$ and $\mu-$, which is lower than 10 %. It will be found that the values of K for the negative corona are always higher than those of the positive corona for the same inter-electrode spacing. The ratio $K-/K+\approx\mu-/\mu+=1.097$ confirms consequently that the mobility of the negative charge carriers is always higher than those of the positive charge carriers.

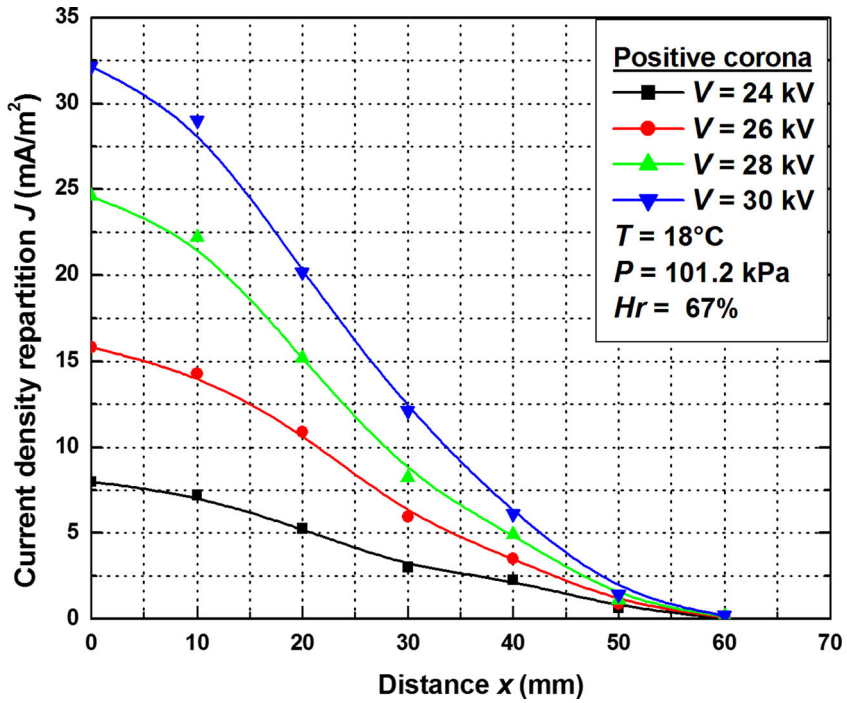

Fig. 12 Current density distribution with various radial distances (x) at different applied voltages for positive corona

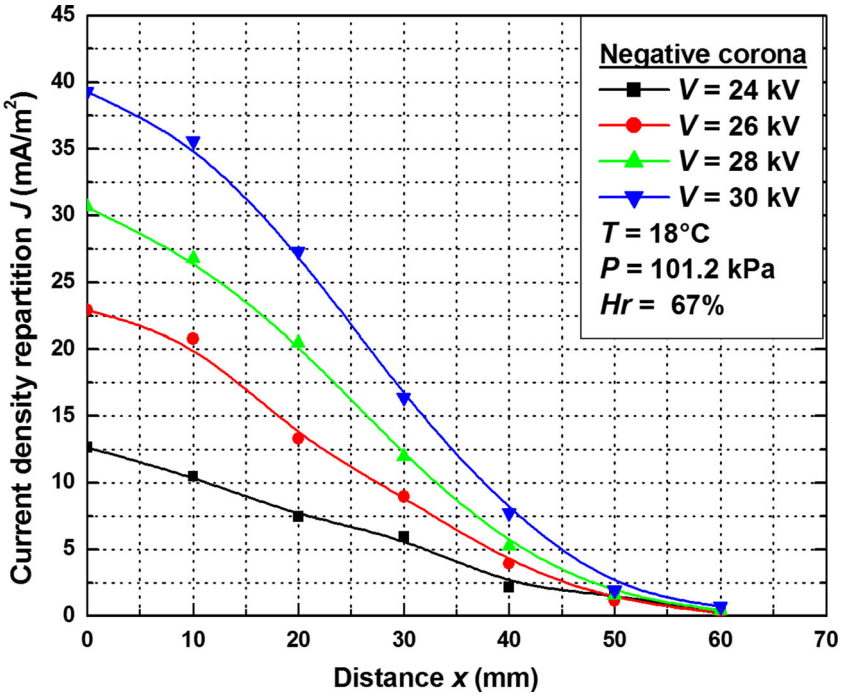

Fig. 13 Current density distribution with various radial distances (x) at different applied voltages for negative corona

4.3 Current Density Distribution Measurements

Figure 12 shows the measured current density distribution on the plane from a positive corona. One can obtain the normalized distribution by dividing the current density values at any position by the on-axis value J_0. The on-axis current density values were J_0=8, 15.83, 24.58, and 32.17 mA/m^2, for V=24, 26, 28, and 30 kV, respectively. The corresponding current density distribution for negative polarity is shown in Fig. 13. The on-axis current densities obtained for this case were J_0=12.67, 22.93, 30.64, and 39.3 mA/m^2, for V=24, 26, 28, and 30 kV, respectively. During these tests, the existing relative air density was δ= 1, with typical temperature, relative humidity, and pressure

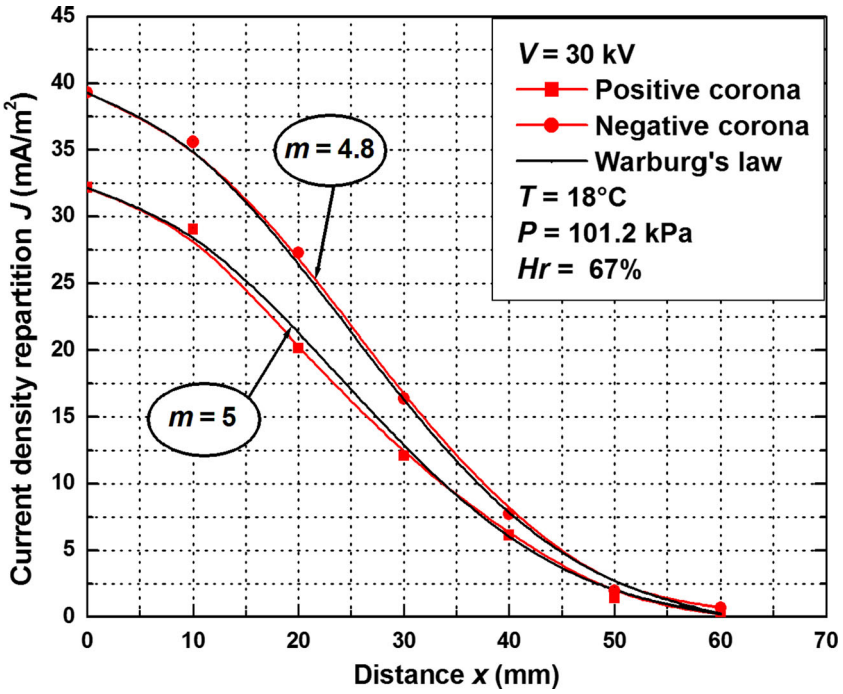

Fig. 14 Profile of Warburg's law and current density distribution for both corona discharges with radial distance (x), at V=30 kV

readings of 18 °C, 67 %, and 101.2 kPa, respectively. Current density was then obtained by dividing the measured current by the surface of the probe.

Figure 14 shows that the Warburg distribution is satisfied and provides an exponent m=5.0 for the positive polarity and an exponent m=4.8 for the negative polarity.

5 Conclusion

The measurement of current-voltage characteristics is the best way to characterize the blade-to-plane electrode configuration, with respect to their use in different applications of the corona discharge. These characteristics can be useful to dimension the high-voltage generator used in the experimental device, but we cannot predict the electric field distribution and the ionic charge that the electrode can produce. This justifies the interest of an experimental study of the current distribution on the surface of the collector electrode. In this work, the corona discharge in a blade-to-plane electrode system has been studied experimentally.

It has been shown that the discharge in a blade-to-plane electrode configuration has the form of the Townsend's discharge law. This was confirmed from the linearity of the conductance corona parameters. The inception corona voltage remained variable for both corona discharges, and the breakdown voltage and also remained practically variable with varying inter-electrode distance.

With this electrical distribution mechanism, the streamer mechanism is possible and dominates at greater distances between the electrodes.

A new general formula developed by Meng et al. to uncover phenomena in point-to-plane geometry corona discharges can also be applied in blade-to-plane system where the exponent n is in the range of 1.5 to 2.0.

To obtain a maximum current, the blade electrodes should be separated from each other by a distance of about $2a \geq h$, confirming the Cooperman's law, under the condition of Eq. (9). So, to obtain a constant value of current, the blade electrodes should be separated by a distance of $2a >> h$, confirming the Cooperman's law, under the condition of Eq. (8).

The values of K or μ for the negative corona were always higher than those for the positive corona. The ratio $\mu-/\mu+>1$ confirmed therefore that one component of the negative charge carriers in the drift region was formed by electrons, of which the mobility is higher than those of ions.

The corona current distribution on the plane was shown to follow Warburg's distribution, given by Eq. (4), providing a value of 5.0 which is used for exponent m in the case of positive polarity. For negative polarity, m=4.8 gives a good fit with the experimental results in the lower half of the distribution. This is consistent with previous research.

Acknowledgments The author would like to thank the staff of High Voltage laboratory, Bejaia University, for their help in carrying out this work.

References

1. I. Yamamoto, H.R. Velkoff, J. Fluid Mech. **108**, 1–18 (1981)
2. N. Zouzou, E. Moureau, G. Touchard, J. Electrost. **64**, 537–542 (2006)
3. P. Molinié, J. Electrost. **45**, 265–273 (1999)
4. A. Tilmatine, S. Flazi, K. Medles, Y. Ramdani, L. Dascalescu, J. Electrost. **61**, 21–30 (2004)
5. N.L.B. Schei, *Electrophotography and Development Physics* (Springer, Berlin, 1989)
6. B. Yahiaoui, B. Tabti, M. Megherbi, A. Antoniu, M.C. Plopeanu, L. Dascalescu, IEEE Trans. Dielectr. Electr. Insul. **20**, 1516–1522 (2013)
7. H. Nouri, M. Aissou, H. Ait Said, Y. Zebboudj, Int. J. Numer. Model. **28**, 138–154 (2015)
8. H. Ait Said, M. Aissou, H. Nouri, Y. Zebboudj, J. Electr. Syst. **10**, 392–405 (2014)
9. L. Zhao, K. Adamiak, J. Electrost. **63**, 337–350 (2005)
10. J.D. Cobine, *Gaseous Conductors* (Dover, New York, 1958)
11. P. Atten, J.L. Coulomb, B. Khaddour, IEEE Trans. Magn. **41**, 1193–1196 (2005)
12. X. Meng, H. Zhang, J. Zhu, J. Phys. D. Appl. Phys. **41**, 065209 (2008)
13. K. Yamada, J. Appl. Phys. **96**, 2472 (2004)
14. H. Nouri, N. Zouzou, E. Moreau, L. Dascalescu, Y. Zebboudj, J. Electrost. **70**, 20–24 (2012)
15. M. Aissou, H. Ait Said, H. Nouri, Y. Zebboudj, Eur. Phys. J. Appl. Phys. **61**, 30803 (2013)
16. J. Podliński, A. Berendt, J. Mizeraczyk, IEEE Trans. Dielectr. Electr. Insul. **20**, 1481–1488 (2013)
17. Y. Zebboudj, G. Hartmann, Eur. Phys. J. Appl. Phys. **7**, 167–176 (1999)
18. B. Khaddour, P. Atten, J.L. Coulomb, IEEE Trans. Magn. **43**, 1193–1196 (2007)
19. M. Townsend, *Electricity in Gases*. (Oxford University Press, 1915)
20. L.B. Loeb, *Electric Coronas—Their Basic Physical Mechanisms* (University of California Press, Berkeley, 1965)
21. B.L. Henson, J. Appl. Phys. **15**, 52709 (1981)
22. G.F.L. Ferreira, O.N. Oliveira, J.A. Giacometti, J. Appl. Phys. **59**, 30–45 (1986)
23. P. Cooperman, Trans. AIEE **79**, 47–50 (1960)
24. E. Warburg, Wied. Ann. **67**, 69–83 (1899)
25. M. Hara, N. Hayashi, K. Shiotsuki, M. Akazaki, IEEE Trans. Power Appar. Syst. **4**, 803–814 (1982)
26. F. Carreno, J. Phys. D. Appl. Phys. **27**, 21362144 (1994)
27. Y. Zebboudj, IEE Proc. Sci. Meas. Technol. **147**, 74–80 (2000)
28. H. Ait Said, H. Nouri, Y. Zebboudj, J. Electrost. **73**, 19–25 (2015)
29. F.W. Peek, *Dielectric Phenomena in High Voltage Engineering* (McGraw-Hill Press, New York, 1921)
30. J. Mi, S. Du, G. Yuan, Curr. Appl. Phys. **12**, 1005–1010 (2012)

31. R. Tirumala, Y. Li, D.A. Pohlman, D.B. Go, J. Electrost. **69**, 1–7 (2010)
32. B.Y. Guo, J. Guo, A.B. Yu, J. Electrost. **72**, 301–310 (2014)
33. H. Ait Said, H. Nouri, Y. Zebboudj, Eur. Phys. J. Appl. Phys. **67**, 30802 (2014)
34. A. Küchler, Hochspannungstechnik Grundlagen - Technologie – Anwendungen. Springer: 3 Neu Bearbeitete Auflage (2009)
35. B.M. Smirnov, Theory of gas discharge plasma. Springer Ser. At. Opt. Plasma Phys. **84**, 229–232 (2015)